

## Pressure dependence of the *Imma* phase of silicon

M. I. McMahon, R. J. Nelmes, N. G. Wright, and D. R. Allan

*Department of Physics and Astronomy, The University of Edinburgh, Mayfield Road, Edinburgh, EH9 3JZ, United Kingdom*

(Received 4 January 1994; revised manuscript received 4 April 1994)

A detailed structural study of the newly observed orthorhombic phase of silicon (space group *Imma*) has been made using angle-dispersive powder-diffraction techniques and an image-plate area detector. The *Imma* phase is found to be stable between 13.2(3) and 15.6(3) GPa, and both the  $\beta$ -tin-to-*Imma* and *Imma*-to-simple-hexagonal transitions are found to be first order with volume changes ( $\Delta V/V_0$ ) of 0.2(1)% and 0.5(1)%, respectively. The volume discontinuities at the transitions are accompanied by pronounced discontinuities in  $\Delta$ , the atomic coordinate of the *Imma* phase, which is found to vary from  $\sim 0.3$  to  $0.4$  over the stability range of the *Imma* phase.

### I. INTRODUCTION

The high-pressure behavior of silicon continues to attract the most attention among the semiconductors. Diffraction measurements have been performed at pressures up to 248 GPa, and until recently ten polymorphs were known to exist. The long-accepted phase transition sequence on compression is cubic diamond (Si-I) to  $\beta$ -tin (Si-II) at  $\sim 11$  GPa,<sup>1-3</sup>  $\beta$ -tin to simple hexagonal (Si-V) at  $\sim 13$ -16 GPa,<sup>2,3</sup> simple hexagonal (SH) to an intermediate phase (Si-VI) at 37.6 GPa,<sup>2</sup> intermediate phase to hcp (Si-VII) at 42 GPa,<sup>2</sup> and hcp to fcc (Si-X) at 78 GPa.<sup>4</sup> The crystal structure of the intermediate phase is uncertain, despite several attempts to solve this long-standing problem.<sup>5,6</sup> On pressure release, the metastable BC8 (Si-III) phase is obtained on slow pressure release from the  $\beta$ -tin phase,<sup>7</sup> while two tetragonal phases (Si-VIII and Si-IX) are obtained on very rapid pressure release.<sup>8</sup> Si-IV, which is thought to have the hexagonal-diamond structure (see Ref. 9), can be obtained by heating BC8-Si at ambient pressure.<sup>10</sup>

Stimulated by the extensive experimental research, the high-pressure behavior of silicon has also been the subject of a large number of theoretical studies.<sup>11</sup> These have been concerned primarily with understanding the relative stability of the various structures through total-energy calculations, while band-structure calculations have predicted correctly that the high-pressure phases of silicon would be superconducting.<sup>12</sup> More recent calculations have predicted the structural pressure dependence of the metastable BC8 phase,<sup>13,14</sup> and the phonon spectra of the high-pressure phases.<sup>11</sup>

Recently, we reported an orthorhombic phase of silicon (space group *Imma*) existing between the  $\beta$ -tin and SH phases.<sup>15</sup> Comparison of the  $\beta$ -tin, *Imma*, and SH phases is simplified if they are all described in terms of a common orthorhombic cell, with the geometrical relationship shown in Fig. 1. The *Imma* structure becomes the  $\beta$ -tin structure when  $a = b$  and  $\Delta = 0.25$ , and becomes the SH structure when  $b/c = \sqrt{3}$  and  $\Delta = 0.50$ . The possibility of an intermediate orthorhombic phase has been considered previously in theoretical calculations,<sup>16,17</sup> and its existence explains the wide range of transition pres-

ures reported for the  $\beta$ -tin to SH transition.<sup>4</sup> The *Imma* phase may also account for the previously unexplained behavior of the superconducting transition temperature  $T_c$  in the range 10-16 GPa.<sup>18-21</sup> Very recently, Lewis and Cohen have performed *ab initio* calculations on the *Imma* phase,<sup>22</sup> and have found the energy of the orthorhombic structure to be lower than, or equal to, the  $\beta$ -tin and SH structures for all unit-cell volumes. Predictions were also made as to the pressure dependence of the lattice-parameter ratios  $c/a$  and  $b/a$ , and the variable atomic coordinate  $\Delta$ .

In this paper we report a detailed structural study of the *Imma* phase of silicon using angle-dispersive powder-diffraction techniques and an image-plate area detector. The range of stability of the *Imma* phase has been determined, and the pressure dependence of the atomic volume, lattice parameters, and variable atomic coordinate have been measured.

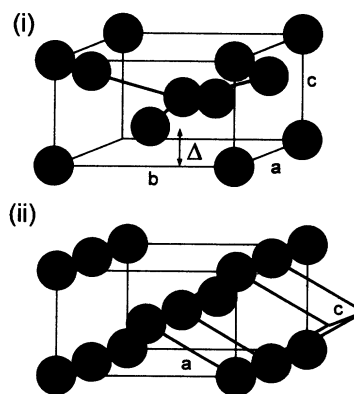


FIG. 1. (i) The *Imma* structure of silicon, with atoms in the  $4(e)$  special positions. The origin chosen here has been moved  $(0, -\frac{1}{4}, -\Delta/2)$  from its standard position to facilitate comparison with the structures of Si-II and Si-V: when  $a = b$  and  $\Delta = 0.25$ , the *Imma* structure is equivalent to the  $\beta$ -tin structure (Si-II), while if  $b/c = \sqrt{3}$  and  $\Delta = 0.50$ , the *Imma* structure is equivalent to the SH structure (Si-V). This latter case is illustrated in (ii), where the standard hexagonal cell is shown for comparison.

## II. EXPERIMENTAL DETAILS

Diffraction data were collected on station 9.1 at the Synchrotron Radiation Source, Daresbury, using angle-dispersive diffraction techniques and an image-plate area detector. The incident wavelength was 0.4654(1) Å. The two-dimensional powder patterns collected on the image plates were read on a Molecular Dynamics 400A PhosphorImager and then integrated to give conventional one-dimensional diffraction profiles. Details of our experimental setup and pattern integration program have been reported previously.<sup>23–25</sup> The sample was a finely ground powder prepared from starting material of 99.9999% purity supplied by the Aldrich Chemical Company.

A Diacell DXR-4 diamond-anvil pressure cell,<sup>26</sup> having a full conical aperture of 50° half angle, was used. The diamond anvils had 600- $\mu\text{m}$ -diam culets, and the preindented tungsten gasket had a spark-eroded hole 150  $\mu\text{m}$  in diameter. The incident beam was collimated by a platinum pinhole to a diameter of 75  $\mu\text{m}$ . Great care was taken to reduce background levels and to avoid parasitic scatter from the gasket. Samples were loaded with a 4:1 mixture of methanol:ethanol as the pressure-transmitting medium, and the pressure was measured to  $\pm 0.1$  GPa using the ruby-fluorescence technique.<sup>27</sup> It was not possible to achieve satisfactory Rietveld refinements of mixed-phase patterns, and so, for consistency, lattice parameters were determined throughout by least-squares refinement of the measured  $2\theta$  values (and hence  $d$  spacings) of the observed reflections. For single-phase *Imma* patterns, the value of  $\Delta$  was obtained from Rietveld refinement<sup>28</sup> of the full integrated profiles using the program MPROF.<sup>29</sup> Two further  $\Delta$  values for mixed-phase *Imma*-SH patterns were obtained by inspection, as described later.

## III. RESULTS AND DISCUSSION

The measured lattice parameter of silicon at ambient pressure was 5.430(1) Å. On compression, the  $\beta$ -tin phase was first observed at 11.7 GPa, in good agreement with the transition pressure of 11.3(2) GPa observed previously for a sample under hydrostatic conditions.<sup>30</sup> The lattice parameters of the diamond and  $\beta$ -tin phases obtained at 11.7 GPa were  $a = 5.256(1)$  Å, and  $a = 4.665(1)$  Å and  $c = 2.565(3)$  Å, respectively. The  $c/a$  ratio for the  $\beta$ -tin phase is thus 0.550, with which the theoretical value of 0.549 agrees well,<sup>22</sup> and the measured volume change ( $\Delta V/V_0$ ) at the diamond-to- $\beta$ -tin transition is 21.0(1)%. A least-squares fit of a Murnaghan equation of state to our compressibility data for the diamond phase gives  $B_0 = 99.9(2.1)$  GPa and  $B' = 3.8(4)$ , in excellent agreement with the values of  $B_0 = 97.88$  GPa and  $B' = 4.23$  obtained from elastic constant measurements.<sup>31</sup>

On further pressure increase, diffraction profiles containing a mixture of the diamond and  $\beta$ -tin phases were observed up to 13.4 GPa. After increasing the pressure to 14.4 GPa, peaks from only the *Imma* phase were observed. Figure 2(i) shows an *Imma* profile (subsequently) collected at a pressure just above the  $\beta$ -tin-to-*Imma* transition. The transition is characterized by the splitting of the (200) reflection of the tetragonal  $\beta$ -tin phase into the distinct (200)<sub>o</sub> and (020)<sub>o</sub> reflections of the orthorhombic

*Imma* phase, as illustrated in the inset. It would clearly be very difficult to determine whether this profile contains a component of the (very similar)  $\beta$ -tin pattern, but the transition does appear to be discontinuous. This is discussed further below. The splitting of (200)<sub>o</sub> and (020)<sub>o</sub> increases with pressure, as illustrated in Fig. 2(ii); comparison of the inset with Fig. 2(i) shows that the (200)<sub>o</sub> reflection moves to lower  $2\theta$  angles, indicating that the  $a$  lattice parameter increases with pressure, while the relatively high compressibility of the  $b$  lattice parameter is revealed by the large shift in the (020)<sub>o</sub> reflection to higher angles. The splittings of (101)<sub>o</sub> and (011)<sub>o</sub>—shown in the inset—(211)<sub>o</sub> and (121)<sub>o</sub>, and (301)<sub>o</sub> and

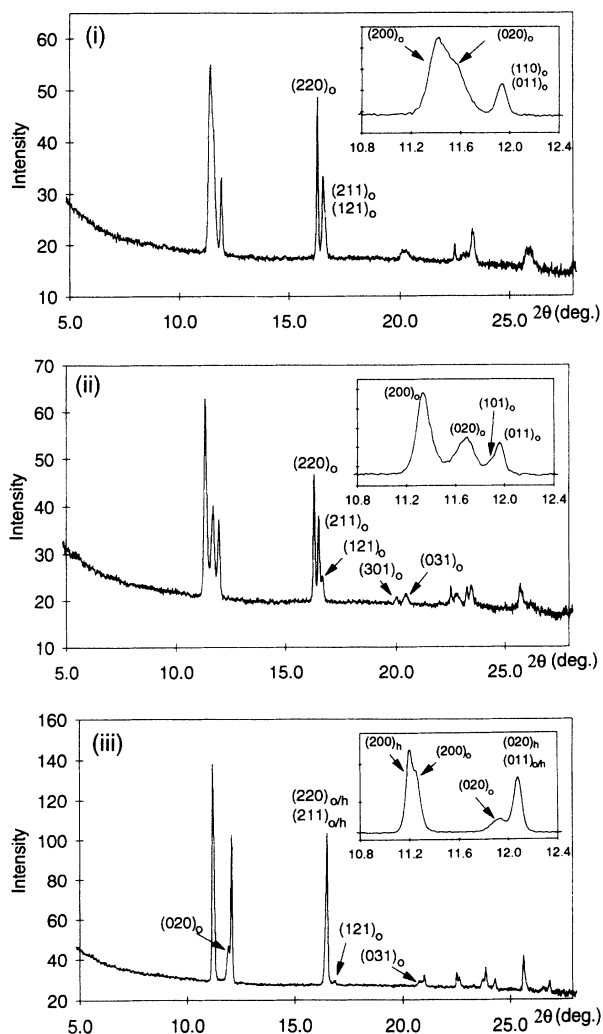


FIG. 2. Integrated profiles of powder-diffraction patterns recorded from silicon (i) at 13.5 GPa, just above the  $\beta$ -tin-to-*Imma* transition, (ii) at 13.9 GPa, well into the stability field of the *Imma* phase, and (iii) at 15.4 GPa, part way through the transition from *Imma* to the simple-hexagonal phase. Some reflections are labeled with their  $(hkl)$  indices, and subscripts "o" and "h" to denote the orthorhombic (*Imma*) and hexagonal phases, respectively. (220)<sub>o/h</sub> denotes the (220)<sub>o</sub> and (220)<sub>h</sub> reflections overlapping too closely to be resolved—and similarly for (211)<sub>o/h</sub> and (011)<sub>o/h</sub>. The insets show the lowest-angle group of reflections in more detail.

(031)<sub>o</sub> also become apparent. The *Imma* phase remained stable until 15.4 GPa, when lines from the SH phase began to appear, as illustrated in Fig. 2(iii). One characterizing feature of the mixed-phase *Imma*-SH profile is the closely spaced low-angle doublet comprising the (200)<sub>o</sub> and (200)<sub>h</sub> reflections from the *Imma* and SH phases, respectively. Also the (020)<sub>o</sub> reflection has moved closer to—but not yet reached—the (011)<sub>o</sub> reflection, which is overlapped by the (020)<sub>h</sub>/(011)<sub>h</sub> reflections of the SH phase. And the splitting of (211)<sub>o</sub> and (121)<sub>o</sub> has increased such that (211)<sub>o</sub> almost coincides with (220)<sub>o</sub>, and they are overlapped by the (211)<sub>h</sub>/(220)<sub>h</sub> reflections to form a nearly symmetric, single, composite peak. The clear differences in  $2\theta$  between (200)<sub>h</sub> and (200)<sub>o</sub>, and between (020)<sub>h</sub> and (020)<sub>o</sub>, show directly that the transition is discontinuous. [The (101)<sub>o</sub> and (301)<sub>o</sub> reflections are not shown in Fig. 2 (iii); they have become too weak to observe.] A least-squares fit to the measured  $d$  spacings of the two phases gives lattice parameters of  $a = 2.553(1)$  Å and  $c = 2.382(1)$  Å for the simple-hexagonal phase [ $a = 4.764(1)$  Å,  $b = 4.422(1)$  Å, and  $c = 2.553(1)$  Å in the orthorhombic setting], and  $a = 4.737(1)$  Å,  $b = 4.479(2)$  Å, and  $c = 2.552(3)$  Å for the *Imma* phase. The volume change ( $\Delta V/V_0$ ) at the *Imma*-to-SH transition is thus 0.5(1)%.

An increase in pressure to 16.2 GPa resulted in a pattern predominantly from the SH phase although a small fraction of the *Imma* phase still remained. The SH lattice parameters at this pressure are  $a = 2.549(1)$  Å and  $c = 2.383(1)$  Å [ $a = 4.766(1)$  Å,  $b = 4.415(1)$  Å, and  $c = 2.549(1)$  Å in the orthorhombic setting]. The  $c/a$  ratio for the SH phase (in the orthorhombic setting) is 0.535, in excellent agreement with the value of 0.533 observed previously<sup>15</sup> and with the theoretical value of 0.534.<sup>22</sup>

After increasing the pressure further to 16.6 GPa, it was decreased. The *Imma* phase first appeared at 15.9 GPa, resulting in a mixed-phase *Imma*-SH pattern. A very small SH component still remained at 15.1 GPa but at pressures below that entirely single-phase *Imma* patterns were obtained down to 13.2 GPa. At 12.7 GPa, the sample had reverted to  $\beta$ -tin. After decreasing the pressure to 12.1 GPa to ensure that the sample contained only the  $\beta$ -tin phase, the pressure was again increased, and data were collected at a further six pressures up to 18.1 GPa, the highest pressure reached in this study. Single-phase *Imma* patterns were obtained from 13.5 up to 15.2 GPa, where a very small SH component first appeared, and single-phase SH patterns were obtained above 16.3 GPa. From all these observations, we conclude that the *Imma* phase is stable from 13.2(3) to 15.6(3) GPa, and note that this stability range corresponds very closely to the wide range of pressures previously assigned to the  $\beta$ -tin-to-SH transition.<sup>4</sup>

The pressure dependences of the  $a$ ,  $b$ , and  $c$  lattice parameters in the  $\beta$ -tin, *Imma*, and SH phases (all in the orthorhombic setting) are shown in Fig. 3, and the corresponding volume compression  $V/V_0$  is shown in Fig. 4. Although it was not possible to detect mixed-phase  $\beta$ -tin-*Imma* patterns, and thus make a direct determination of the relative densities at the same pressure, the  $V/V_0$

data suggest that the  $\beta$ -tin-to-*Imma* transition is first order with a volume change  $\Delta V/V_0$  at 13.2 GPa of 0.2(1)%. Thus about 50% of the 1.4% change in atomic volume between the  $\beta$ -tin and SH phases occurs at the  $\beta$ -tin-to-*Imma* and *Imma*-to-SH transitions.

A volume discontinuity of  $\sim 0.2\%$  would also seem to occur within the *Imma* phase at  $\sim 15$  GPa (Fig. 4), and inspection of Fig. 3 reveals that this is a result principally of a discontinuity in the  $b$  lattice parameter. However,  $\sim 15$  GPa is the upper pressure at which single-phase *Imma* patterns were observed, and above this only mixed-phase *Imma*-SH patterns occurred. We believe that the apparent discontinuity in the unit-cell volume of the *Imma* structure is an artifact of the mixed-phase nature of the samples, with the *Imma* unit cell being “stretched” towards the shape required in the SH phase. We have seen similar unit-cell distortions in mixed-phase samples of InSb (Ref. 32) and CdTe.<sup>33</sup> With this in mind it is probably incorrect to determine the volume change at the *Imma*-to-SH transition from the mixed-phase sample obtained at 15.4 GPa. However, the alternative procedure of extrapolating the SH equation-of-state to 15 GPa gives the same volume change of 0.5(1)%.

The pressure dependence of the variable atomic coordinate  $\Delta$  in the *Imma* structure is shown in Fig. 5. Six full refinements of single-phase *Imma* patterns were possible, two on profiles collected on pressure increase and four on profiles collected on pressure decrease. As well as  $\Delta$  and

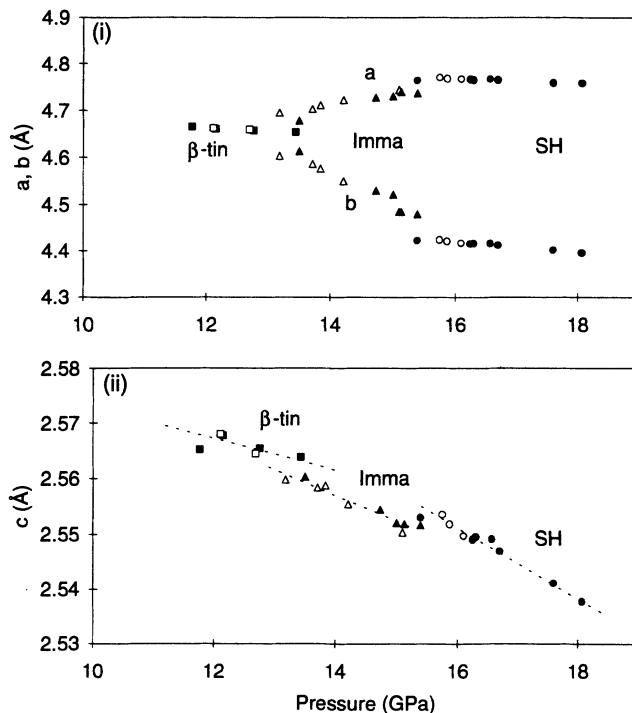


FIG. 3. The pressure dependence of (i) the  $a$  and  $b$  lattice parameters, and (ii) the  $c$  lattice parameter, of the  $\beta$ -tin (■ and □), *Imma* (▲ and △), and simple hexagonal (● and ○) phases of silicon—all referred to the common orthorhombic unit cell shown in Fig. 1(i). The points shown as solid symbols were obtained on pressure increase, and those shown as open symbols were obtained on pressure decrease.

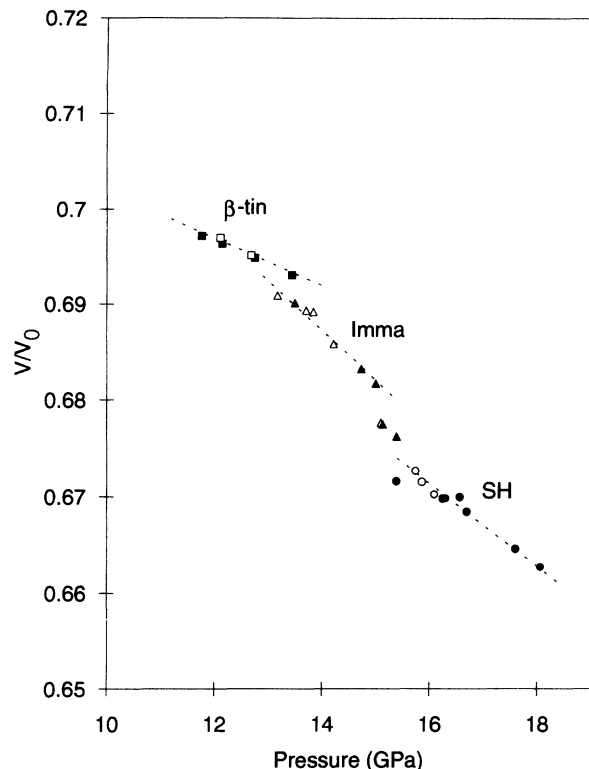


FIG. 4.  $V/V_0$  as a function of pressure for the  $\beta$ -tin (■ and □), *Imma* (▲ and △), and simple hexagonal (● and ○) phases of silicon, where  $V$  and  $V_0$  are volumes per atom and the measured value of  $V_0$  in the diamond phase at ambient pressure is  $20.01 \text{ \AA}^3$ . Points shown as solid symbols were collected on pressure increase, and those shown as open symbols were collected on pressure decrease. The dotted lines are guides for the eye.

the lattice parameters, four peak-width parameters and a scale factor, these refinements included a variable preferred-orientation (PO) parameter which showed a strong PO effect around the [001] direction—more pronounced for the profiles collected on pressure increase. The accuracy of the structural refinements was limited to some extent both by the  $hkl$ -dependent peakwidths observed in the *Imma* phase, and by correlations between  $\Delta$  and the (strong) preferred orientation, but the six points clearly indicate that  $\Delta$  does not vary continuously from  $\Delta = \frac{1}{4}$  to  $\Delta = \frac{1}{2}$  in the *Imma* phase. Rather, the results suggest that the discontinuities in atomic volume are accompanied by possibly even more pronounced discontinuities in  $\Delta$  at both the  $\beta$ -tin-to-*Imma* and *Imma*-to-SH transitions. Because of the similarity of the  $\beta$ -tin pattern and the patterns obtained from the *Imma* phase just above the  $\beta$ -tin-to-*Imma* transition [Fig. 2(i)], it is not possible to show conclusively from lattice-parameter measurements alone that this transition is discontinuous: the changes in  $V/V_0$  and the  $c$  lattice parameter appear to be discontinuous, while the splitting of the  $a$  and  $b$  lattice parameters [Fig. 3(i)] could be continuous. However, the results obtained for  $\Delta$  give a stronger indication of discontinuity.

There is no doubt about the discontinuous nature of

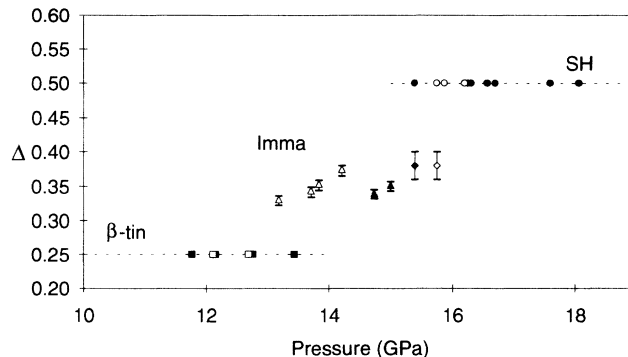


FIG. 5. The pressure dependence of the atomic coordinate  $\Delta$  in the  $\beta$ -tin (■ and □), *Imma* (see below), and simple hexagonal (● and ○) phases of silicon. In the  $\beta$ -tin phase,  $\Delta$  is fixed by symmetry at 0.25, while in the simple hexagonal (SH) phase it is fixed at 0.5—referred to the common orthorhombic unit cell shown in Fig. 1(i). Points shown as ▲ and △ are from single-phase *Imma* samples, while those shown as ◆ and ◇ are from mixed-phase *Imma*-SH samples. Solid and open symbols distinguish results obtained on pressure increase and decrease, respectively.

the *Imma*-to-SH transition, as shown by the peak splittings already discussed in the mixed-phase *Imma*-SH profile of Fig. 2(iii). Further evidence can be obtained from the value of  $\Delta$  for such mixed-phase profiles, collected on both pressure increase and decrease above 15 GPa. Although it was not possible to perform full Rietveld analysis on these profiles, a determination of  $\Delta$  could be made from the relative intensities of the (020), (121), and (031) reflections from the *Imma* phase [see Fig. 2(iii)]. The (121) reflection is absent in the SH phase and strong in the  $\beta$ -tin phase, and so its intensity is strongly dependent on  $\Delta$ . This reflection is clearly visible in the mixed *Imma*-SH profile in Fig. 2(iii), collected on pressure increase at 15.4 GPa. From the intensity of (121) relative to (020) and (031)—and assuming the preferred orientation to remain similar to that obtained from the full refinements of the single-phase patterns— $\Delta$  can be estimated as 0.38(2). Thus, even at a pressure at which the sample has mostly transformed to the SH phase, the value of  $\Delta$  is very significantly different from  $\Delta = 0.5$ . Performing a similar analysis on a mixed-phase sample collected at 15.8 GPa on pressure decrease again yields  $\Delta = 0.38(2)$ . These two points are plotted in Fig. 5 using ◆ and ◇ for data collected on pressure increase and pressure decrease, respectively. Although some uncertainties remain as to precise values due to the effects of strong preferred orientation, our results show that  $\Delta$  varies only from  $\sim 0.3$  to 0.4 over the stability range of the *Imma* phase. As for the atomic volume, this represents only  $\sim 50\%$  of the difference between the  $\beta$ -tin and *Imma* phases—probably less in this case (see Fig. 5).

The discontinuous nature of the  $\beta$ -tin-to-*Imma* and *Imma*-to-SH transitions, and the small range of stability of the *Imma* phase, from  $V/V_0 \sim 0.69$  to 0.68, differ from the behavior predicted by the recent calculations of Lewis and Cohen.<sup>22</sup> Their results indicate continuous transitions, with the *Imma* phase having an energy lower than

or equal to those of the other two phases over a wide range of  $V/V_0$  from  $\sim 0.80$  to  $0.63$ . They discuss some possible reasons for this discrepancy, including the effect of finite temperature.<sup>22</sup> It is to be noted that the calculations show  $\Delta$  varying only from  $\sim 0.34$  to  $0.37$  over the actual range of stability of the *Imma* phase<sup>22</sup>—in approximate agreement with the observed behavior (see Fig. 5).

On the basis of continuous transformations. Lewis and Cohen question our previous suggestion<sup>15</sup> that the  $\beta$ -tin-to-*Imma* and *Imma*-to-SH transitions might account for the discontinuities reported in the superconducting transition temperature  $T_c$  at similar pressures.<sup>18–21</sup> But the observed discontinuous character of the transitions keeps this possibility open.

In summary, our main conclusions are as follows.

(1) An orthorhombic *Imma* phase is confirmed to exist, on both pressure increase and pressure decrease, between the  $\beta$ -tin and simple-hexagonal (SH) phases of silicon. The stability range of the *Imma* phase is 13.2(3)-15.6(3) GPa.

(2) The  $\beta$ -tin-to-*Imma* and *Imma*-to-SH transitions are both found to be discontinuous in character, with volume

discontinuities of 0.2(1) and 0.5(1)%, respectively.

(3) The volume discontinuities at the  $\beta$ -tin-to-*Imma* and *Imma*-to-SH transitions are accompanied by discontinuities in  $\Delta$ , the variable atomic coordinate of the *Imma* phase, which is found to vary from  $\sim 0.3$  to  $0.4$  (with increasing pressure) over the stability range of the *Imma* phase.

#### ACKNOWLEDGMENTS

We gratefully acknowledge the assistance of our colleague J. S. Loveday in various aspects of the experimental work, and Dr. S. P. Lewis and Professor M. L. Cohen for making a copy of Ref. 22 available prior to publication. We also had a helpful discussion with Professor Cohen. We would like to thank A. A. Neild and G. Bushnell-Wye of the Daresbury Laboratory for their help in preparing the beam-line equipment, and Professor E. Sinn of Hull University for the loan of one of the pressure cells. This work was supported by a grant from the Science and Engineering Research Council and by facilities made available by Daresbury Laboratory. Valued assistance with the maintenance and development of pressure cells has been given by D. M. Adams of Diacell Products.

- 
- <sup>1</sup>J. C. Jamieson, *Science* **139**, 762 (1963).  
<sup>2</sup>H. Olijnyk, S. K. Sikka, and W. B. Holzapfel, *Phys. Lett.* **103A**, 137 (1984).  
<sup>3</sup>J. Z. Hu and I. L. Spain, *Solid State Commun.* **51**, 263 (1984).  
<sup>4</sup>S. J. Duclos, Y. K. Vohra, and A. L. Ruoff, *Phys. Rev. Lett.* **58**, 775 (1987).  
<sup>5</sup>S. J. Duclos, Y. K. Vohra, and A. L. Ruoff, *Phys. Rev. B* **41**, 12 021 (1990).  
<sup>6</sup>V. Vijaykumar and S. K. Sikka, *High Pressure Res.* **4**, 306 (1990).  
<sup>7</sup>J. S. Kasper and S. M. Richards, *Acta Crystallogr.* **17**, 752 (1964).  
<sup>8</sup>Y. X. Zhao, F. Buehler, J. R. Sites, and I. L. Spain, *Solid State Commun.* **59**, 679 (1986).  
<sup>9</sup>R. J. Nelmes, M. I. McMahon, N. G. Wright, D. R. Allan, and J. S. Loveday, *Phys. Rev. B* **48**, 9883 (1993).  
<sup>10</sup>R. M. Wentorf, Jr., and J. S. Kasper, *Science* **139**, 338 (1963).  
<sup>11</sup>S. P. Lewis and M. L. Cohen, *Phys. Rev. B* **48**, 3646 (1993), and references therein.  
<sup>12</sup>K. J. Chang and M. L. Cohen, *Phys. Rev. B* **30**, 5376 (1984).  
<sup>13</sup>J. Crain, S. J. Clark, G. J. Ackland, M. C. Payne, V. Milman, P. D. Hatton, and B. Reid, *Phys. Rev. B* **49**, 5329 (1994).  
<sup>14</sup>S. J. Clark, G. J. Ackland, and J. Crain, *Phys. Rev. B* **49**, 5341 (1994).  
<sup>15</sup>M. I. McMahon and R. J. Nelmes, *Phys. Rev. B* **47**, 8337 (1993).  
<sup>16</sup>K. J. Chang and M. L. Cohen, *Phys. Rev. B* **31**, 7819 (1985).  
<sup>17</sup>R. J. Needs and R. M. Martin, *Phys. Rev. B* **30**, 5390 (1984).  
<sup>18</sup>M. A. Il'ina and E. S. Itskevich, *Fiz. Tverd. Tela (Leningrad)* **22**, 3139 (1980) [*Sov. Phys. Solid State* **22**, 1833 (1980)].  
<sup>19</sup>K. J. Chang, M. M. Dacorogna, M. L. Cohen, J. M. Mignot, G. Chouteau, and G. Martinez, *Phys. Rev. Lett.* **54**, 2375 (1985).  
<sup>20</sup>T. H. Lin, W. Y. Dong, K. J. Dunn, C. N. J. Wagner, and F. P. Bundy, *Phys. Rev. B* **33**, 7820 (1986).  
<sup>21</sup>J. M. Mignot, G. Chouteau, and G. Martinez, *Phys. Rev. B* **34**, 3150 (1986).  
<sup>22</sup>S. P. Lewis and M. L. Cohen, *Phys. Rev. B* **48**, 16 144 (1993).  
<sup>23</sup>R. J. Nelmes, P. D. Hatton, M. I. McMahon, R. O. Piltz, J. Crain, R. J. Cernik, and G. Bushnell-Wye, *Rev. Sci. Instrum.* **63**, 1039 (1992).  
<sup>24</sup>R. O. Piltz, M. I. McMahon, J. Crain, P. D. Hatton, R. J. Nelmes, R. J. Cernik, and G. Bushnell-Wye, *Rev. Sci. Instrum.* **63**, 700 (1992).  
<sup>25</sup>R. J. Nelmes and M. I. McMahon, in *Proceeding of the 42nd Annual Conference on Applications of X ray Analysis, Denver 1993*, edited by C. S. Barrett (Plenum, New York, in press).  
<sup>26</sup>D. M. Adams, Diacell Products, 54 Ash Tree Road, Leicester, UK.  
<sup>27</sup>G. F. Piermarini, S. Block, J. D. Barnett, and R. A. Forman, *J. Appl. Phys.* **46**, 2774 (1975).  
<sup>28</sup>H. M. Rietveld, *J. Appl. Crystallogr.* **2**, 65 (1969).  
<sup>29</sup>A. N. Fitch and A. D. Murray (unpublished).  
<sup>30</sup>J. Z. Hu, L. D. Merkle, C. S. Menoni, and I. L. Spain, *Phys. Rev. B* **34**, 4679 (1986).  
<sup>31</sup>H. J. McSkimin and P. Andreatch, Jr., *J. Appl. Phys.* **35**, 2161 (1964).  
<sup>32</sup>R. J. Nelmes, M. I. McMahon, P. D. Hatton, J. Crain, and R. O. Piltz, *Phys. Rev. B* **47**, 35 (1993).  
<sup>33</sup>M. I. McMahon, R. J. Nelmes, N. G. Wright, and D. R. Allan, *Phys. Rev. B* **48**, 16 246 (1993).